Behaviour of Li isotopes during regolith formation on granite (Massif Central, France): Controls on the dissolved load in water, saprolite, soil and sediment

Philippe Négrel, Romain Millot

BEHAVIOUR OF LI ISOTOPES DURING REGOLITH FORMATION ON GRANITE (MASSIF CENTRAL, FRANCE): CONTROLS ON THE DISSOLVED LOAD IN WATER, SAPROLITE, SOIL AND SEDIMENT

NÉGREL, Ph., MILLOT, R.

BRGM, Laboratories Division, Orléans, France -- p.negrel@brgm.fr,

Abstract

Lithium (Li) contents and isotopes were studied in all environments of a small river catchment draining granite in the Margeride mountains of the French Massif Central. This covered surface waters, primary and accessory minerals of the granites, the whole rock, and soil and sediment samples developed in the catchment, completed with regional data for mineral waters and rainwater. The integrated investigation aimed at evaluating the potential of Li isotopes as effective tracers of water/rock interaction processes within a granitic environment. The δ^7Li values and Li concentrations were measured on sediment- and soil samples, following standard acid-dissolution procedures and chemical purification of Li using the cationic exchange resin protocol in a clean lab. Lithium-isotope compositions were measured with a Neptune MC-ICP-MS and Li concentrations by ICP-MS. The samples represented different stages of granite weathering, including fresh granite, weathered-rock, surface saprolite, and sediments in riverbanks and fields bordering the streams. The extent of Li mobility during granite weathering was first evaluated through determining the percentage change relative to Ti, with a range from -31 to -66% in the collected samples. The weathered-rock was depleted by -47% for Li with negative δ^7Li values ranging from -1.9 to -3.4‰. Soil to riverbank sediment samples were characterized by less negative δ^7Li values, indicating that Li is enriched in soil with fractionation of Li isotopes and changes of the mineral abundance in the samples. To complement this first view, we i) Modelled the theoretical Li isotope signature of water interacting with granite, using a weathering model based on dissolution; ii) Applied an atmospheric-input correction to surface waters; iii) Applied a Raleigh equation for modelling the Li isotope fractionation when compared with corrected surface water and mineral water; and iv) Compared Li isotopes with Sr-isotope data in a larger weathering framework.

Keywords: weathering, isotopes, lithium, groundwater, soil, sediment, granite

1 – Introduction

Continental silicate weathering is one of the major processes controlling the chemical evolution of the Earth's surface (Gaillardet et al., 1999), because crystalline basement rocks represent over 50% of the earth's terrestrial surface (Amiotte Suchet et al., 2003). Weathering leads to the formation of unconsolidated alterite or saprolite, usually representing a thickness of up to several tens of metres (Velbel, 1988). The study of alteration processes combines the use of several tools, such as geochemistry (e.g., Nesbitt and Markovics, 1980), isotopic tracing (e.g., Négrel et al., 2018), mineralogy (e.g., Braga et al., 2002), and the notions of space and scale, ranging from a small watershed (White and Blum, 1995; Ackerer et al., 2016) to continental river basins like the Amazon, Ganges or Congo basins (Gaillardet et al., 1999; Abbas and Subramanian, 1984; Négrel et al., 1993).

The links and relationships between weathering, development of saprolite on hill slopes and large-scale dissolved-load transport by streams are very complex. Despite the existence of numerous tools for studying weathering processes (e.g., isotopes of Sr, U, etc.), the increasing need for proxies has underpinned the development of chemical—such as rare earth elements—and isotopic tools, such as lithium and, more recently, silicon, calcium and magnesium (see Sullivan et al., 2016, for synthesis).

Lithium has two stable isotopes of mass 6 and 7, with natural abundances of 7.5% and 92.5%, respectively; it is a mobile element that tends to incorporate into the fluid phase during water/rock interactions. The relative mass difference between the two isotopes is considerable at 17%, generating significant mass-dependant fractionation during geochemical processes. Tomascak (2004) noted that the range of variation in lithium-isotope compositions is over 50‰ in geological materials. Silicate rocks have Li-isotope compositions ranging from –2 to +10‰ (Coplen et al., 2002; Teng et al., 2004). The Li isotope of seawater is about +31‰ (Millot et al., 2004); river water has a large range (-6.0 to +32.2‰, Huh et al., 1998); and (saline) thermo-

60 mineral water generally has isotopic compositions of 0 to +15‰ (Millot and Négrel, 2007;
61 Millot et al., 2010b).

62 In the context of water/rock interactions, numerous studies have clearly shown that Li
63 isotopes are a promising proxy for tracing silicate weathering reactions (e.g. Huh et al., 1998,
64 2001; Pistiner and Henderson, 2003; Kisakurek et al., 2004; Rudnick et al., 2004; Pogge von
65 Strandmann et al., 2012; Millot et al., 2007, 2010a, 2010b; Vigier et al., 2009; Wang et al.,
66 2015; Clergue et al. 2015). Silicate minerals host Li and chemical weathering induces isotopic
67 fractionation. This results in enrichment of the heavy isotope (^{7}Li) in solution, the light isotope
68 (^{6}Li) being preferentially retained in secondary weathering mineral phases (Huh et al., 2004;
69 Vigier et al., 2008; Weynell et al., 2017), similar to other non-traditional stable-isotope systems
70 such as Ca, Fe and B (Sullivan et al., 2016). Today, lithium isotopes are applied to a wide range
71 of geochemical processes, such as weathering (Pistiner and Henderson, 2003; Huh et al., 2004;
72 Hathorne and James, 2006; Lemarchand et al., 2010; Wanner et al., 2017; Wimpenny et al.,
73 2010; Ryu et al., 2015; Pogge von Strandmann et al., 2019). Other applications are to the study
74 of erosion processes, either in large river-basin studies (Huh et al., 1998, 2001; Kisakurek et
75 al., 2005; Millot et al., 2010a; Dellinger et al., 2015; Henchiri et al., 2014; 2016; Wang et al.,
76 2015; Murphy et al., 2019), or in smaller streams (Vigier et al., 2009; Pogge von Strandmann
77 et al., 2010; Liu et al., 2015); to studying anthopogenic disturbance in soils (Négrel et al., 2010;
78 Tsai et al., 2014); and as geothermometer proxies in mineral waters (Millot and Négrel, 2007),
79 or for tracing groundwater flowpaths (Négrel et al., 2012; Pogge von Strandmann et al., 2014).
80 However, studies on granitic bedrock and its associated weathering products are very scarce
81 (Rudnick et al., 2004; Lemarchand et al., 2010).

82 At the basic scale of a watershed, the challenge is to integrate all the reservoirs and parts
83 of the watershed affected by the weathering processes. This has been the case in studies
84 involving classic tools, such as strontium isotopes, but not when working with newly developed

85 tools. In this study, we measured lithium and its isotope values in all reservoirs and parts of a
86 catchment draining granite. This included surface- and mineral waters, primary minerals and
87 accessory phases of the granites, the whole rock, and samples of soil and sediment generated
88 within the watershed, completed with additional data for rainwater.

89 Our study has used Li-isotope data for tracing silicate weathering processes at the basic
90 scale of a watershed, considering all its components. This is a novel approach for Li isotopes,
91 which earlier were partly limited due to the difficulty of collecting and analysing samples from
92 all reservoirs. This systematic work is part of a long-term, wide-ranging and integrated
93 geochemical study covering major and trace elements, Sr isotopes, Nd isotopes and rare earth
94 elements, in water, sediment and soil within the Margeride mountains of central France (Négrel,
95 1999; 2006; Négrel et al., 2000); this also includes incorporation of all relevant outside data,
96 such as on separated minerals and long-term monitoring of rainfall.

97 Isotopic investigation of weathering products generally provides good information on
98 the chemical reactions taking place during such processes. This is further demonstrated by
99 recent studies on the Li isotope systematics of silicate-rock weathering, in complement to
100 investigations covering regolith production and the development of weathering profiles
101 (Vázquez et al., 2016; Ackerer et al., 2016).

102 In order to apply Li isotopes as effective tracers of water/rock interaction processes in a
103 small mono-lithological catchment, the effect of atmospheric input was investigated to correct
104 the lithium values of surface- and mineral waters. This allowed replacing Li isotopes with Sr
105 isotopes in a larger weathering framework. We also tested a steady-state weathering model and
106 fractionation process modelling on the Margeride granite-gneiss, prerequisites for our reactive-
107 transport model computer simulations that coupled a large number of chemical reactions with
108 mass transport, a key challenge for the effective use of Li isotopes as a tool in weathering
109 studies.

2 - General setting

The granite-gneiss Margeride massif is located in the south of the French Massif Central (Figs. 1a, b). It consists of light and dark granite-gneiss with an average mineral composition of the light facies of 37% quartz, 30% oligoclase, 23% K-feldspar and 10% biotite, and of 31% quartz, 30% andesine, 20% K-feldspar and 19% biotite in the dark facies (Marchand et al., 1985). The mineralogy and chemistry of Margeride granite and gneiss are similar, although the relative abundance of minerals may fluctuate slightly. The presence of a micaschist unit in the massif is worth noting, composed of quartz, muscovite and biotite. Couturié et al. (1979) reported that the different facies of the Margeride granite (323±12 Ma., Rb-Sr isochron) resulted from fractional crystallization of a crustal magma in a subhorizontal laccolith. The Desges River, a tributary of the Allier, flows approximately 40 km between the upper part of the Margeride massif and its confluence with the Allier (Négrel, 1999; Fig. 1b). The watershed covers 89 km^2 and ranges in altitude from 1250 m (headwaters) to 650 m (outlet); the dense N-S-oriented drainage pattern mainly on the top of the Margeride plateaus receives an average annual precipitation of 1000 to 1200 mm/yr^{-1}.

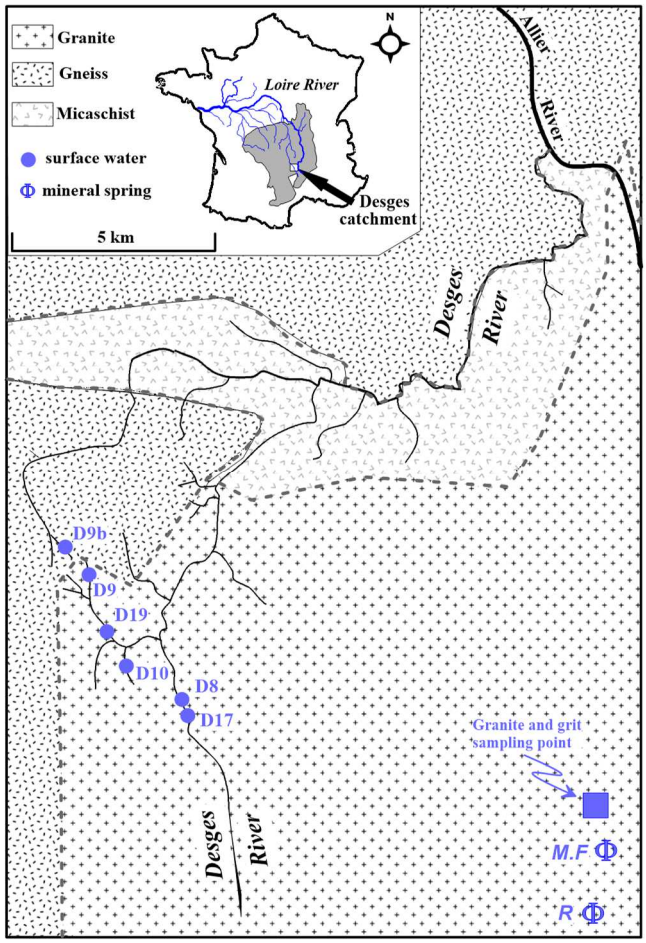

Figure 1. General location map of the Massif Central (in blue-grey), and detailed map of the Desges watershed showing the sampling sites, modified from Négrel (1999; 2006). The main geological units are granite, gneiss, and micaschist. The different sampling points are: bedrock and granitic grit of the Desges watershed, mineral springs (Mazel and Fontaine Basses (M.F) and Ranc (R), surface waters, soils and sediments (Dx).

3 – Material and methods

In a temperate climate, granite usually weathers into grit (Sequeira Braga et al., 1990; 2002; Le Pera et al., 2001; Paquet and Clauer, 2012). Unweathered bedrock and granitic grit were collected at the same place (Fig. 1, blue square). The Mazel grit sample, collected on top of a granite outcrop, has a fabric skeleton structure retaining the original granitic one, which is commonly observed in the lower (45-100 cm depth) part of the soil profile here. Although the texture of the parent rock was largely preserved, the main transformations are chloritization of biotite, kaolinization of plagioclase, and the presence of oxy-hydroxides (Sarazin, 1979). This is reflected in our sample that is mainly composed of quartz (20%), K-feldspar (20%),

140 plagioclase (20%) and chlorite (5%), and for which we adopt the classification of Begonha and
141 Sequeira Braga (2002) as “weathered rock”.

142 Samples A0, A1 and A2 were collected around station D17, and samples B0, B1 and B2
143 around station D19 (Fig. 1). A0 and B0 (Négrel, 2006), collected from a weathering profile, are
144 not a direct skeleton-fabric material of the granite, but are surface saprolite mainly composed
145 of sand and silt. Samples A1 and B1 are riverbank sediments, classified as sandy-silt. All four
146 samples mainly consist of quartz, K-feldspar, plagioclase and illite-micas, with dramatic
147 changes in relative abundances (Négrel, 2006).

148 The soils in this catchment are podzol and peat, varying in thickness from a few
149 centimetres at the top of the profile to a few metres farther down. They mainly consist of
150 kaolinite, hydroxides and vermiculite, K feldspar and biotite (isolated from the matrix), and
151 ubiquitous organic and amorphous phases (Bourrié, 1978; Sarazin, 1979). Soil samples A2 and
152 B2, collected in fields bordering the streams, can be classified as silty-sand and contain small
153 amounts of quartz, K-feldspar, plagioclase and illite-micas.

154 The sample-preparation procedure was described in detail by Negrel and Deschamps
155 (1996) and Négrel (1999; 2006). Briefly, weathered rock (Mazel) and surface saprolite (A0 and
156 B0) were powdered, the other soil and sediment samples being oven-dried at 70 °C,
157 homogenized, quartered and dry-sieved through a 165 µm nylon mesh, and powdered before
158 analysis. The δ^7Li values were measured on the sediment- and soil samples following standard
159 acid-dissolution. For rock and sediment, total sample digestion was necessary before separation
160 of Li from the matrix. About 50 mg of crushed sample was dissolved in a closed beaker with
161 an ultrapure mixture of three acids [4 ml HF (23N), 1 ml HNO_3 (14N) and 0.1 ml $HClO_4$ (12N)]
162 for four days at 100 °C. After this, once the acid mixture had evaporated, 4 ml of HCl (6N) was
163 added for four days at 100 °C. A sample aliquot (30 ng of Li) of the acid-dissolution residue

was then dissolved in 0.5 ml of HCl (0.2N) before being placed in a column containing cationic resin for Li separation.

Surface-water samples were collected from the river according to the protocol in Négrel (1999); groundwater samples were thermo-mineral waters from naturally flowing springs, taken according to the protocol in Négrel (2006). Briefly, water samples were collected in the field in acid-washed polyethylene bottles after filtration through 0.2 µm Sartorius® cellulose acetate filters and then acidified to pH <2, by adding ultra-pure HNO_3.

Lithium isotopic compositions in soil, sediment and water were measured with a Neptune MC-ICP-MS (see Millot et al., 2004, for details) and Li concentrations with a quadrupole ICP-MS. The $^7Li/^6Li$ values were normalized to the L-SVEC standard solution (NIST SRM 8545) following the standard-sample bracketing method. Typical in-run precision on δ^7Li determination was about 0.1-0.2‰ ($2\sigma_m$). Chemical separation of lithium from the matrix was achieved before mass analysis following a procedure adapted by Millot et al. (2004), using cationic resin (Bio Rad AG® 50W-X12, 200-400 mesh) and HCl (0.2N) for 30 ng of lithium. Blanks for total chemical extraction were less than 20-30 pg of Li, which is negligible since the blank/sample ratio is less than 10^{-3}. Accuracy and reproducibility of the total method (purification procedure plus mass analysis) were tested by repeated measurements of a seawater standard (IRMM BCR-403) after separation of Li from the matrix, for which we obtained a mean value of δ^7Li = +30.8‰±0.4 (2σ, n=15) over the duration of the analytical period. This mean value agrees with our long-term measurements (δ^7Li = +31.0‰±0.5, 2σ, n=30, Millot et al. 2004) and with other values from the literature.

4 – Results

The Li data (δ^7Li and Li contents) of rock, grit, soil, sediment and separate minerals from the granite and surface and groundwater collected in the catchment are given in Table 1.

Sample	Ref.	Li ppm	δ7Li		Sample	Ref.	Li	δ7Li
							µmol L-1	
M1/POU	Whole rock	143.1	-1.9		*Spring waters*			δ7Li
ALT1	Mazel grit	104.7	-3.4		Mazel		551	5.0
					FB1		424	4.9
Ap	Apatite	13.3	0.0		Ranc1		158	3.8
Pl	Plagioclase	20.9	-1.7		Ranc2		397	2.6
Bi	Biotite	489.1	0.8					
KF	K-Feldspar	5.3	-2.6		*Surface waters*			
					D10'		0.22	12.7
D19-3/A0	A0	56.2	0.1		D8		0.15	9.2
D19-3/A1	A1	68.8	-2.1		D11		0.23	12.1
D19-3/A2	A2	110.9	-3.4		D9bis		0.16	10.0
D17-3/B0	B0	60.6	3.3		D9'		0.21	10.7
D17-3/B1	B1	61.6	0.0		D11'		0.24	13.0
D17-3/B2	B2	66.2	-2.7					

Table 1. Results of Li concentration ($\mu g\ g^{-1}$) and δ^7Li for parent rock, grit, separate minerals, sediment and soil, expressed in ppm. Results of Li concentration ($\mu g\ g^{-1}$) and δ^7Li for thermo-mineral waters (e.g., saline waters cold on surface, but linked to a deep hot reservoir) from Millot and Négrel, 2007; results of Li concentration ($\mu mol\ l^{-1}$) and δ^7Li for surface waters.

For the separate minerals, Li-rich phases decreased in content from biotite (489 µg g^{-1}) to K-feldspar (5 µg g^{-1}), for an average whole-rock Li content of about 143 µg g^{-1}. Lithium isotopic compositions in the separate minerals ranged from -2.6‰ in K-feldspar to 0.0‰ in apatite, for a δ^7Li of -1.9‰ in bulk rock. Reconstituting the whole rock from the separate minerals led to a Li content of 56 µg g^{-1} and a δ^7Li of 0.45‰. These values are inconsistent with the measured ones, implying that the rest of the Li probably occurs in residual minerals with a Li content of around 86.6 µg g^{-1} and a δ^7Li of -3.43‰. The Li content in soil and sediment fluctuated from 56 µg g^{-1} (surface saprolite A0) to 111 µg g^{-1} (soil A2). With the exception of soil A2 (almost twice the content in soil B2), the samples had similar Li contents (surface saprolite 56 *vs.* 61 µg g^{-1}; sediment samples 69 *vs.* 62 µg g^{-1}). Li isotopes in soil and sediment samples ranged from -3.38‰ (soil A2) to 3.31‰ (surface saprolite B0).

Surface waters in the catchment had a roughly constant Li content of around 0.14 to 0.24 µmol L^{-1}, corresponding to the lower value observed in streams draining volcanic rocks in the Massif Central, (Table 1), whose range of variation is from 0.4 to 2.35 µmol L^{-1} (Négrel et al., 2010a). Li-isotope compositions (δ^7Li) varied in the catchment (Table 1), ranging from +9 to +12‰, which is lower than that in other water samples from the Massif Central (Négrel et

al., 2010) that range from +12 to +15.1‰. Lithium-isotope compositions and Li concentrations in the surface waters have a linear relationship (δ^7Li = 5.36 x Li + 3.73), with a correlation coefficient r^2 = 0.81 (n=6). For groundwater, the lithium concentrations and δ^7Li were published by Millot et al. (2007): Li concentrations ranged from 157 µmol L^{-1} (Ranc 1) to 547 µmol L^{-1} (Mazel; their Table 3), which is one order of magnitude higher than in surface water and consistent with their data for thermo-mineral waters in the Massif Central. Lithium-isotope compositions (δ^7Li) in these groundwaters were less variable (+2.6 to +5.0‰) than in surface waters, with the lowest value observed in Ranc 2 (+2.6‰) and the highest in Mazel (+5‰), a range of variation similar to that in thermo-mineral waters of the Massif Central (δ^7Li from +2.6 to +5.5‰, Millot et al., 2007).

5 – Discussion

5.1. Mobility of Li during weathering

In order to evaluate the extent of the chemical mobility of Li during granite weathering, we calculated the weathering intensity with τ, the elemental mass transfer coefficient of Brimhall and Dietrich (1987). This calculation avoids the dilution effect and impact of volume change due to weathering (Nesbitt, 1979). We thus calculated the percentage change for Li relative to the immobile element Ti (Clergue et al., 2015) with equation (1), previously used for other elements in the same catchment (Négrel, 2006) and according to Nesbitt (1979):

$$\tau_{Li} = 100 \times ([(Li/Ti)_{sample}/(Li/Ti)_{granite}] - 1) \qquad \text{(Equation 1)}$$

Expressed as a percentage, $\tau = 0$ represents the initial unweathered material and τ = -100% means complete removal of Li from the parent material. A positive value reflects Li enrichment by concentration in residual minerals and negative values represent Li depletion, lost from bedrock because of its solubility. However, compared to other soluble elements, less

depletion of Li may be related to its incorporation into secondary minerals. The percentage change of Li in the samples, i.e. loss or gain of mobile Li relative to immobile Ti (τ_{Li}, Fig. 2), ranges from -31 to -66% , the extreme values being for surface-saprolite samples (A0, B0). The grit is depleted around -47% compared to bedrock, with a decrease of the δ^7Li value and a Li content from -1.9‰ and 143.1 µg g^{-1} in granite to -3.4‰ and 104.7 µg g^{-1} in grit (Fig. 3). The D19 samples show more Li depletion in surface saprolite (A0, -66%) than in riverbank sediment (A1, -60%) and soil (A2, -46%). This depletion is marked by a continuous decrease of δ^7Li values from +0.1‰ in surface saprolite to -3.4‰ in soil. Compared to the decrease in δ^7Li values, Li concentration remains constant between samples A0 and A1, and shows an increasing trend in soil sample A2 (Fig. 3), which has the same δ^7Li and Li-concentration values as those of the grit.

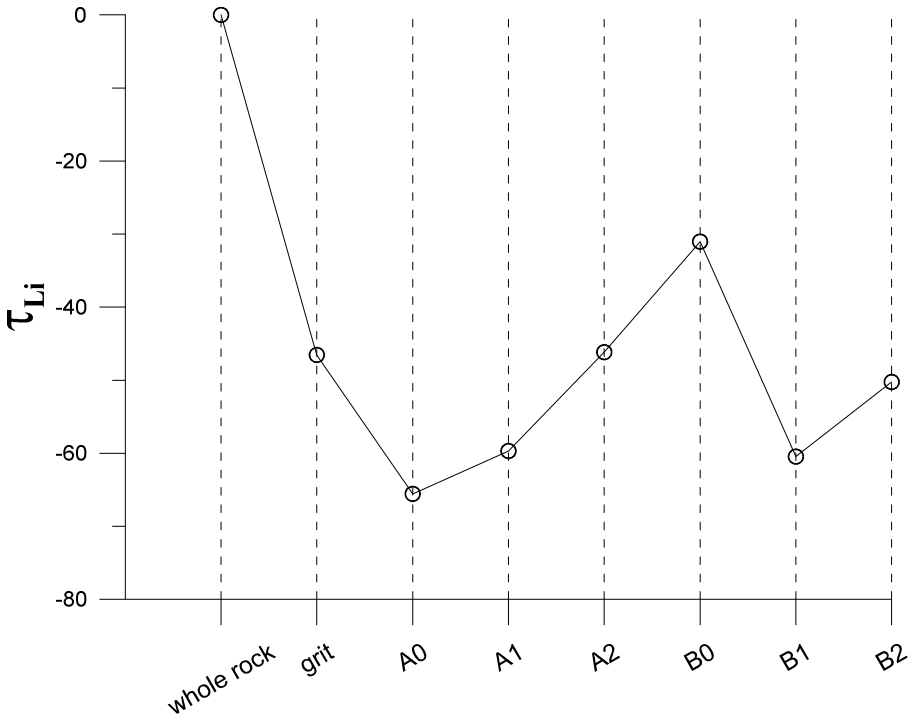

Figure 2. Percentage change of (mobile) Li relative to (immobile) Ti (Equation 1).

The mineralogical composition of the samples was earlier presented in Négrel (2006). Briefly, surface saprolite A0 is composed of quartz (35%), K-feldspar (~20%), plagioclase

(~20%) and illite-micas (~20%). At station D19, riverbank-sediment sample A1 is quite different, with more quartz (50%), less feldspars (5%) and illite-mica around 20%; it is also richer in chlorite (20%). Soil sample A2 contains the least quartz (15-20%); with K-feldspar, illite-micas and plagioclase all around 20%. This variation is accompanied by more negative δ^7Li values, meaning that Li is enriched in soil with a fractionation of Li isotopes and changes in the mineral abundance of the samples (residual minerals have negative δ^7Li; Fig. 3). This is accompanied by a change in the Li concentration, with an 18% increase between A0 and A1, from 56 to 69 µg g^{-1}, and a38% increase between A1 and A2, from 69 to 112 µg g^{-1}. Between saprolite and soil, the Li concentration increases by 50%.

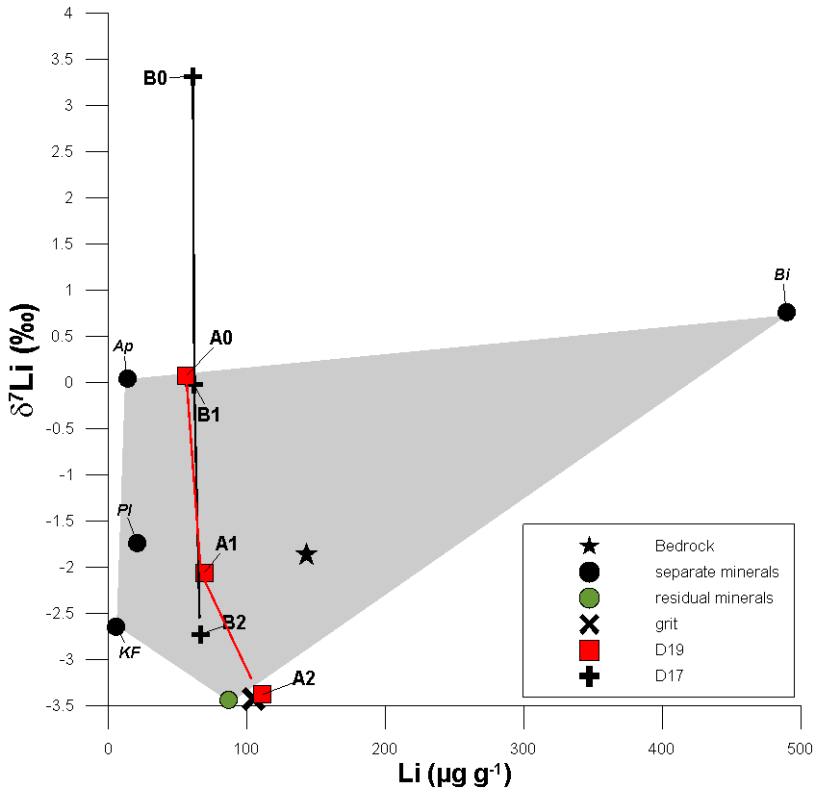

Figure 3. Relationship between δ^7Li values (‰) and Li contents (µg g^{-1}) for bedrock, grit, surface saprolite (A0, B0), riverbank sediments (A1, B1) and soil (A2, B2). The separate minerals from the granite define the greyed area with the addition of residual minerals.

Contrary to station D19, the samples from station D17 show more erratic variations. Surface saprolite B0, depleted around -31%, has a positive δ^7Li value of +3.3‰, clearly higher than all mineral values in the granite. Sediment sample B1 is largely depleted (-60%) with a

268 δ^7Li value close to 0‰. Soil sample B2 is depleted around -50% with a more negative δ^7Li
269 value of -2.7‰. Compared to the significant variation in δ^7Li values, the Li concentration
270 remains largely constant in the three samples with a total variation of around 8% (Fig. 3). Quartz
271 reaches 65% in surface saprolite sample B0, K-feldspar and illite-smectite having a similar
272 abundance (~20%), but plagioclase is only 5%. Riverbank sediment sample B1 contains around
273 25% quartz, and 20% K-feldspar, 20% plagioclase and 20% illite-mica, but only 5% chlorite
274 with 15% as an amorphous phase. Soil sample B2 contains the least quartz (15-20%), but K-
275 feldspar, illite-micas and plagioclase contents are still around 20%. Again, the δ^7Li values
276 become more negative from surface saprolite to soil, which can be explained by changes in
277 mineral abundance in the samples, as higher amounts of residual minerals in the soil sample
278 lead to more negative δ^7Li values.

279 ### *5.2. Atmospheric input correction to surface and groundwater*

280 The need to quantify and subtract the portion of elements contributed by precipitation in the
281 chemical composition of surface- and ground-waters has been apparent for several decades
282 (e.g., Stallard and Edmond, 1981; Meybeck, 1983). Basically, quantifying the precipitation
283 input requires knowledge of its chemical composition (Négrel et al., 1993; Grobois et al., 2000).
284 The classic reference of atmospheric input in unpolluted hydrosystems is chloride, which
285 behaves conservatively throughout the hydrological cycle; the correction for its atmospheric
286 contribution is estimated by reference to the Cl concentration in river water, multiplied by the
287 ratio element/Cl of precipitation (e.g., Meybeck, 1983; Négrel et al., 1993). As stated by Négrel
288 (2006), in the absence of evaporites in the Margeride catchment, Cl ions in the river water can
289 be assumed to originate from wind-blown sea salt and human activity. High Cl contents can be
290 found in (thermo-mineral) groundwater emerging as naturally flowing springs, which are
291 closely related to fractures in the granite that cannot play any role in supplying Cl to the river
292 water. This would have been different in the case of an unexposed basement rock with a cover

293 of sedimentary rock, as described by Négrel et al. (1997). In our mass-balance approach,
294 determining input-output budgets for dissolved constituents in waters similar to Négrel's (2006)
295 work, we used the mean weighted rainfall on the Massif Central over 1.5 years for Cl content
296 (Négrel and Roy, 1998).

297 To determine the highest chloride concentration derived from precipitation input, the
298 standard method (Meybeck, 1983; Négrel et al., 1993) is to multiply the mean weighted Cl
299 value by a concentration factor F resulting from evapotranspiration. With a mean weighted
300 chloride of around 20 µmol L^{-1} and an F value of approximately 1.6, around 32 µmol L^{-1}
301 represent the highest chloride concentration originating from atmospheric input to the river.
302 When the Cl content in water is below 32 µmol L^{-1} (Table 1), the entire chloride content of the
303 river is assigned an atmospheric origin; when it is over 32 µmol L^{-1}, the residual chloride in the
304 river is attributed to human activity (Meybeck, 1983).

305 Using rainwater samples obtained during a rain-input survey over the Massif Central
306 (Négrel and Roy, 1998), Millot et al. (2010b) reported low lithium concentrations, between
307 0.004 and 0.292 µmol L^{-1}, whereas the δ^7Li values varied greatly between +3.2‰ and +95.6‰
308 over the study period. From this observed range, two groups of rainwater with very different Li
309 characteristics were identified (Fig. 4). The first one, named "natural", had a Li concentration
310 of 0.04 µmol L^{-1} with a δ^7Li value of around +6.9‰; the second one, named "anthropogenic",
311 had a Li concentration of 0.13 µmol L^{-1} and a much higher δ^7Li value of around +79‰. For the
312 Li isotopes, considering natural and anthropogenic components, the average value over the
313 1.5 year survey was +26.2‰ and the mean concentration-weighted Li isotopes value was
314 +20.3‰ (Millot et al., 2010b). For correcting Li contents and Li isotopes of surface water from
315 rainfall data, we used the average Li content, 0.06 µmole L^{-1}, and the average δ^7Li, +26.20‰,
316 of all rainwater samples collected in the Massif Central over 1.5 years (Négrel and Roy, 1998;
317 Millot et al., 2010b; Fig. 4).

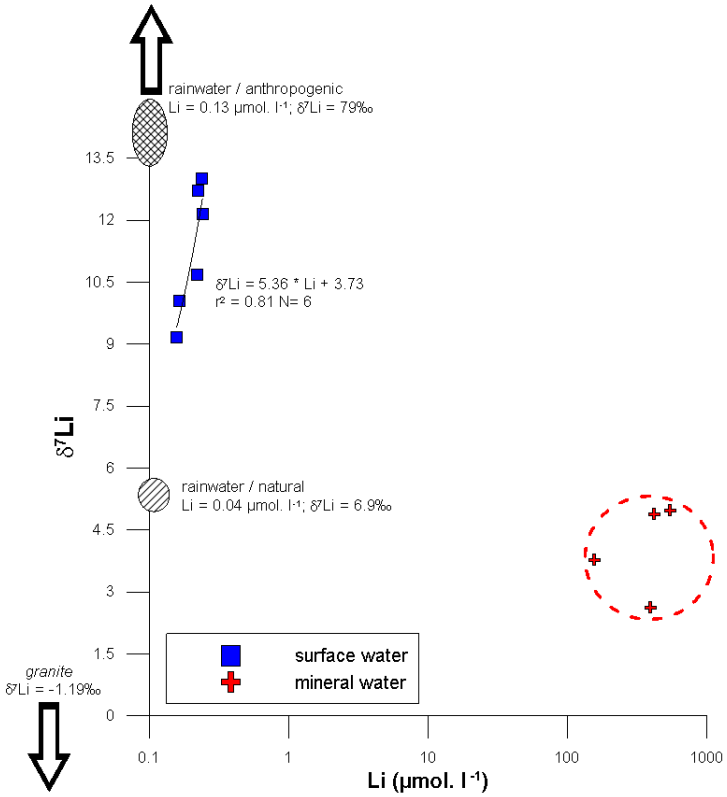

Figure 4. Plot of δ^7Li versus Li concentration (µmol L^{-1}) for surface water, groundwater and rainwater.

Surface-water samples D8, D9', D9b, D10', D11 and D11' were investigated by Négrel (1999; 2006) for anion contents and now, in this study, for Li (Fig. 4). Applying the atmospheric correction to these surface-water samples showed that D9b and D8 derived their total Cl content from precipitation input and thus reflect no anthropogenic influence, with 35% and 61% of the Li deriving from atmospheric input, respectively. This shows a non-negligible influence of precipitation input on the Li budget in this case, contrary to other observations at very different scales by Ryu et al. (2014) in Hawaii, or by Millot et al. (2010) in the Mackenzie Basin of northern Canada.

Other samples have a residual Cl content that is generally related to anthropogenic input, mainly from agricultural activity. Here, the Li derived from atmospheric input ranged from 40% in sample D11 to 43% in samples D9 and D10. Accordingly, as done by Négrel (1999 and 2006) for the same catchment, we corrected the Li-isotope values observed in the water for

335 atmospheric contribution, which gave a δ^7Li ranging from +10.8 (D11') to -2.0‰ (D8). The
336 δ^7Li for samples without residual Cl are the lowest, with a δ^7Li of -2.0‰ for sample D8 and
337 +0.8‰ for sample D9b. A similar atmospheric correction to mineralized waters has a low
338 impact on Li content (less than 0.06% of the Li being from precipitation input) with no change
339 in the δ^7Li value, indicating the dominant influence of water/rock interaction on both Li content
340 and δ^7Li value of the mineralized waters.

341 However, contrary to previous work on atmospheric and anthropogenic corrections to
342 surface-water chemistry (Négrel, 1999; 2006; Petelet-Giraud et al., 2003), we cannot use the
343 same method for anthropogenic-input correction here. The residual Cl after atmospheric
344 correction derives from anthropogenic input and the correction for such input (e.g. to a zero Cl
345 content) requires knowledge of its Li/Cl ratio. However, this ratio cannot be constrained
346 accurately, which would allow a robust correction for Li content and thus for Li isotopes.

347 Applying the atmospheric correction to the D8, D9, D10 and D11 surface water samples
348 (Négrel, 2006), shows that D8 and D9 derived their total Cl content from atmospheric input,
349 and thus reflect no anthropogenic influence. The Sr content derived from atmospheric input is
350 around 50% in D9 and 57% in D8. The influence of atmospheric input on $^{87}Sr/^{86}Sr$ ratios is
351 consistently significant (Négrel, 2006), and, corrected for atmospheric input, the $^{87}Sr/^{86}Sr$ ratios
352 for water–granite interaction range from 0.72316 (D8) to 0.72511 (D9). Once corrected for
353 atmospheric input, the δ^7Li value and Cl concentration are controlled by water–granite
354 interaction and anthropogenic input(s). This is summarized in Fig. 5, where δ^7Li is plotted
355 *versus* residual Cl. The two samples with no residual Cl directly yield the value of the δ^7Li
356 derived from water-rock interaction, with δ^7Li values of +0.8‰ (D9) and -2.0‰ (D8)
357 associated with Li concentrations of 0.11 and 0.06 µmol L^{-1}, respectively. The other samples
358 have residual Cl values from 7.4 (D10) to 49.7 µmol L^{-1} (D11), δ^7Li value from +6.4‰ (D9)
359 to +10.8‰ (D11) and nearly constant Li concentrations of 0.13 to 0.15 µmol L^{-1}. This can be

360 related to an increase of the anthropogenic input, with a roughly constant δ^7Li.

361 Regarding the anthropogenic Li sources, Négrel, et al. (2010) gave a range for the δ^7Li
362 in fertilizers, such as carbonaceous amendment or NPK, between +2.1‰ and +215‰ and a
363 mean weighted δ^7Li value of +14.2‰. For Li used with other trace elements, such as Cu, Fe,
364 Mn, Zn, Co, Mo and B, even though not necessary as an additional nutrient (Négrel et al.,
365 2010a), the δ^7Li ranged between -16‰ and + 31‰ with a mean weighted δ^7Li value of +1.3‰.
366 These two mean values agree with the range observed in surface waters and thus can explain
367 an anthropogenic input from agricultural activities.
368

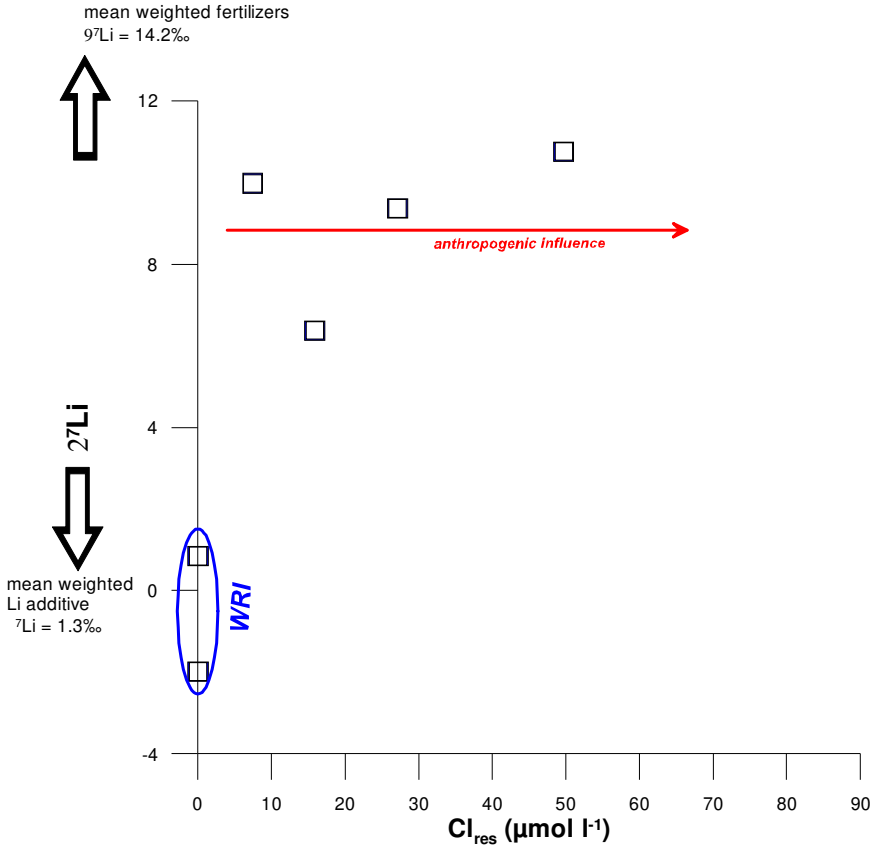

369
370 *Figure 5. Plot of δ^7Li versus the residual Cl concentration (µmol L^{-1}) for surface water, once*
371 *corrected from precipitation input (see text). The mean weighted δ^7Li values for the fertilizers*
372 *and Li additives used in agricultural practices are indicated.*
373

5.3 The weathering model for Li

5.3.1 The simple dissolution model

Négrel et al. (2001) developed a weathering model based on dissolution, giving the theoretical (th) isotopic signature (i) of a chemical element (Z) in water being in equilibrium with granite (iZ_{th}), which was initially developed for and applied to strontium. This model considers the congruent dissolution of Sr-bearing phases (mx), their abundance ($\%_{mx}$), isotope ratio (iZ_{mx}) and element concentration (Z_{mx}). Each mineral characteristic considered (iZ_{mx} and Z_{mx}) is weighted by the weatherability (W_{mx}) of each (Négrel et al., 2001), summarized in equation 2:

$$iZ_{th} = \frac{\sum \left(iZ_{mx} \times Z_{mx} \times \%_{mx} \times W_{mx} \right)}{\sum \left(Z_{mx} \times \%_{mx} \times W_{mx} \right)} \quad \text{(Equation 2)}$$

The theoretical isotopic composition (iZ_{th}) of water in equilibrium with granite was then used for Sr in several environments (Négrel et al., 2001; Petelet-Giraud et al., 2003; Négrel, 2006), before being redefined and applied to Nd and Pb in the present watershed (Négrel, 2006; Négrel et al., 2010b). The initial model was based on the hypothesis that the dissolution of plagioclase, K-feldspar and biotite contributes most elemental Sr. The same set of minerals, plus apatite for Nd, and apatite and allanine for Pb, were then considered (Négrel, 2006; Négrel et al., 2010b). For lead-isotope compositions during granite dissolution, we used the concept of Harlavan and Erel (2002) that highlights the role of accessory phases and primary minerals in controlling the isotope composition during water-rock interaction; for the accessory phases, it was suggested that apatite played a major role. Our model thus assumes that only the fluid concentration changes, the isotopic ratio remaining constant, because the secondary minerals are in equilibrium with the parent solution for Sr, Nd and Pb. The relative mineral weatherability W_{mx}, considering that of plagioclase as 1, is 0.25 for biotite and 0.1 for K-feldspar (Négrel et al., 2001). A sensitivity analysis of the model (Petelet-Giraud et al., 2003b; Négrel, 2006), based on testing various mineral-weatherability values from the literature (Blum

et al., 1994; Zuddas et al., 1995), consistently showed only minor differences in the isotope values. The model was verified for Sr by comparing the iSr_{th} calculation for given conditions of Sr abundance and the isotopic characteristics of separate minerals, with the $^{87}Sr/^{86}Sr$ ratio of water that has interacted with several granitoids and basalts in France (Petelet-Giraud et al., 2003; Négrel, 2006).

For this study, the model was adapted for lithium and applied to the Margeride granite, using data from Table 1. In view of the composition of this granite, we considered K-feldspar, plagioclase and biotite as primary minerals, and apatite as an accessory phase in the model of eq. 2. This was also based on interaction experiments by Millot and Négrel (2013) between a rainwater reference solution (TMRAIN-95) and 1.5 g of powdered granite sample from India at 25 °C (Négrel et al., 2010b). Millot and Négrel (2013) monitored Pb- and Li-isotopic compositions over 12 months of interaction, showing that:

i) When using Pb isotopes, there is a major contribution of K-feldspar and plagioclase dissolution, and, to a lesser extent, of biotite and apatite dissolution;

ii) When using Li isotopes, the light lithium isotope (^6Li) is preferentially retained during uptake of Li into secondary minerals during weathering.

The theoretical δ^7Li signature for water draining this granite is close to -3.3‰. The difference in the isotopic values is always less than 0.1 for Li during sensitivity analysis of the model, done by testing various mineral-weatherability values similar to the Sr, Nd and Pb models (Petelet-Giraud et al., 2003; Négrel, 2006; Négrel et al., 2010b). Our model only provides information on the isotopic value of water after interaction with minerals; it does not assume that the main process associated with isotope fractionation is the formation of secondary precipitates, such as clays, even though the evolution of Li-isotope values is controlled by the precipitation of secondary minerals, as was shown in other environments (Huh et al., 2001; Pistiner and Henderson, 2003; Vigier et al., 2008; Millot et al., 2010).

5.3.2. A broader weathering frame using Li and Sr isotopes: Implications for water/rock interaction in the critical zone

Figure 6 is a plot of the δ^7Li *vs.* ^{87}Sr/^{86}Sr values, where the results from primary minerals and accessory phases of the granites, the whole rock, the soil and sediment samples, and the mineral-water and surface-water samples, are plotted with the results of the weathering-model computation for the granite. The Sr-isotope systematics for primary minerals and accessory phases of the granites, whole rock, soil and sediment samples, and mineral-water data are from Négrel (2006), and those for surface-water samples are from Négrel (1999).

Figure 6 shows several features: 1) For surface waters, the δ^7Li and ^{87}Sr/^{86}Sr values disagree with the weathering model, even if Li is not corrected for atmospheric input, the δ^7Li being either lower or higher than the model value. 2) For thermo-mineral spring waters, there is again no agreement with the results of the weathering model, all springs having a higher δ^7Li than the weathering model, and a larger influence caused by an increase in weathering of one or more minerals cannot explain the values observed for δ^7Li values in the mineralized waters, no minerals in the Margeride granite having such a high δ^7Li value. This is particularly true for the residual trace minerals that cannot control the δ^7Li values of the water (Figs. 3 and 6). For thermo-mineral spring waters, the δ^7Li values thus suggest that other processes lead to the observed signatures because the ^{87}Sr/^{86}Sr ratio agrees with the results of the weathering model. 3) For the residual solids, the ^{87}Sr/^{86}Sr difference between whole rock (0.72269) and Mazel grit (0.73134) reflects the weathering of low ^{87}Sr/^{86}Sr- and Rb/Sr-bearing minerals, such as plagioclase and K-feldspar; this is confirmed by the grit mineralogy (~20% of each in this sample; Négrel, 2006), whereas the Mazel grit shows a depleted δ^7Li compared to the whole rock. 4) Riverbank sediment A1 at site D19 shows an ^{87}Sr/^{86}Sr ratio of 0.74408 and a δ^7Li of 0.1‰, both higher than that of the grit. An increase in the Sr-isotope ratio is noted in the

sediment from surface saprolite A0 ($^{87}Sr/^{86}Sr = 0.75085$) down to soil A2 ($^{87}Sr/^{86}Sr = 0.75290$), accompanied by a large decrease in δ^7Li (from +0.1 to -3.4‰). In site D17, soil B2 has the lowest $^{87}Sr/^{86}Sr$ ratio (0.76296) and δ^7Li (-2.7‰), and, as for site D19, the $^{87}Sr/^{86}Sr$ (0.76649) in sediment B1 collected on the river bank increases to 0.78508 in surface saprolite B0, accompanied by a large increase in the δ^7Li (from 0 to +3.3‰).

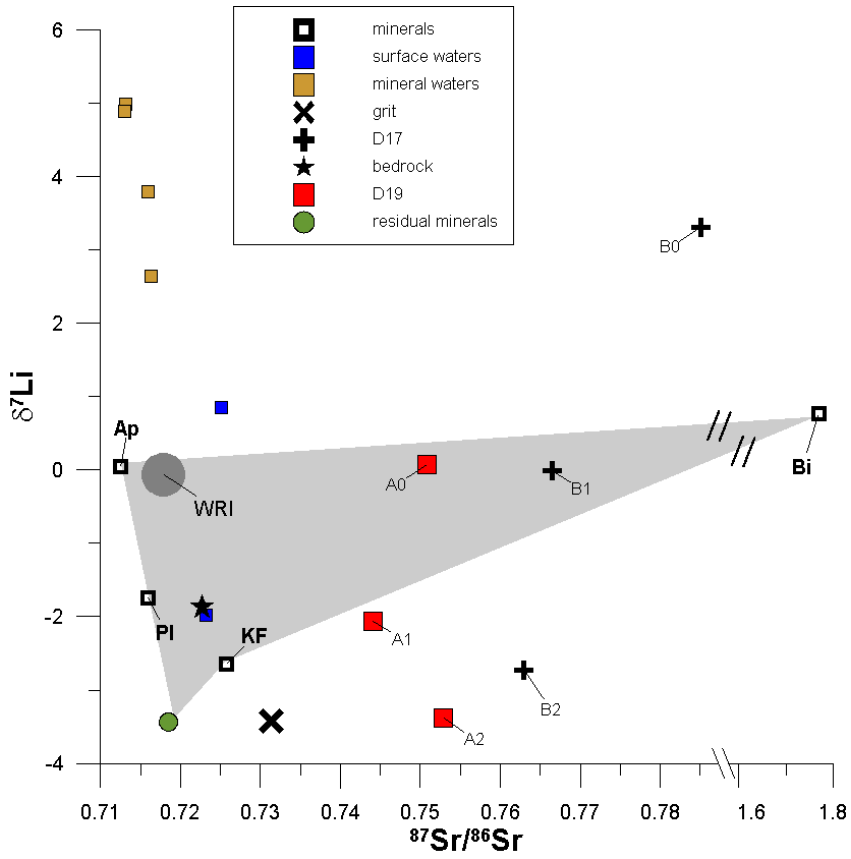

Figure 6. Relationship between the δ^7Li and $^{87}Sr/^{86}Sr$ for Margeride granite, separate minerals and Mazel grit sample, and surface and mineralized spring waters. δ^7Li and $^{87}Sr/^{86}Sr$ of the remaining trace minerals (titanite, rutile, epidote, zircon) are indicated in the graph (see text). The result of the weathering model is indicated by the grey circle (see text). The separate minerals from the granite define the greyed area with the addition of residual minerals.

5.3.3 Modelling Li isotopic fractionation using a Raleigh equation: the role of secondary phase precipitation

Here, we apply the batch fractionation model for Li isotopes as developed by Bouchez et al. (2013) and used by Clergue et al. (2015). This model is based on the non-congruent dissolution of bedrock leading to a δ^7Li in solution ($\delta^7Li_{solution}$). As a first approach, this model is only

based on (non congruent) dissolution/precipitation reactions. The main process occurring in this solution is Li-isotope fractionation through the formation of secondary phases that preferentially incorporate light lithium (^{6}Li). This gives a residual solution with a $\delta^{7}Li_{diss}$ and a $\delta^{7}Li_{sec}$ for the secondary phases. The $\delta^{7}Li_{sec}$ can be expressed as follows:

$$\delta^{7}Li_{sec} = \frac{\alpha \times \delta^{7}Li_{rock} + 1000\, f_{Li}\,(\alpha - 1)}{\alpha\,(1 - f_{Li}) + f_{Li}} \qquad \text{(Equation 3)}$$

The key parameters are the isotope fractionation factor $\delta^{7}Li_{sec}$ between the different secondary minerals, and the solution ($\delta^{7}Li_{solution}$) and proportion ($1\text{-}f_{Li}$) of Li in secondary phases. The f_{Li} can be expressed by the elemental mass transfer coefficient τ calculated with equation (1), which represents the evolution of the Li/Ti ratio in sediment compared to that of bedrock.

The isotope fractionation factor is calculated from chemical and isotope data measured on field material; this can be applied to samples from soil, rivers and the sedimentary record, and does not require prior knowledge of the isotope fractionation factors involved in the detailed reactions. Weathering products are modelled here with a fractionation factor $\alpha_{sec\text{-}dis}$ ranging from 0.975 to 0.998, consistent with the range of α values used in the literature (Rudnick et al., 2004; Clergue et al., 2015). To summarize, the α values in the literature span a range from 0.970 to 1.000 and derive either from laboratory experiments (0.979-0.984, Millot et al., 2010c; Vigier et al., 2008), or from field data (0.982-0.989, Millot et al., 2010a, 2010c; Tipper et al., 2012; Dellinger et al., 2013; 2014; 2015).

We found that the fractionation factor $\alpha_{sec\text{-}dis}$ on Figure 7 can explain some, but not all, weathering products; the lowest $\delta^{7}Li$ observed in the samples fit with the α max (0.998), but no point is explained by the α min (0.975). Thus, we cannot fit the required fractionation factor

488 $\alpha_{sec\text{-}dis}$ to the soil and sediment data (Fig. 7). Additional processes or inputs should thus be
489 considered and investigated.

490 Facing a broader range of isotopic fractionation for the precipitation of secondary phases
491 than the one defined from experimental clay precipitation, Lemarchand et al. (2010) argued for
492 the precipitation of another possible phase with a higher isotope fractionation. As far as we
493 know, no studies have been carried out on such phases, but oxides could be a good candidate
494 for the fractionation of Li isotopes and can account for the existence of high δ^7Li values in
495 weathering products. This argument was already proposed by Millot et al. (2010a) to explain
496 incipient weathering effects on Li isotopes in the Canadian Rocky Mountains. Concerning our
497 samples, only B1 and B2 have an amorphous phase identified by X-ray diffraction (15 and 5%,
498 respectively; Négrel, 2006), agreeing with a δ^7Li shift away from the α max line, but only for
499 B1, as sample B2 plots close to the α max line. Conversely, no amorphous phase was identified
500 in samples A0, A1 and B0, though the δ^7Li is shifted from the α max line. Thus, the
501 precipitation of secondary clay minerals is not enough to explain the δ^7Li shift and the role of
502 other phase-like oxides must be considered.

503 Fe–Mn oxides, one of the main oxides in the non-residue part of soils and river
504 sediments, have an exceptional tendency (particularly Mn oxides) for scavenging trace
505 elements (Cu, Zn, Ni, Pb, etc.; Carpenter et al., 1975), Li not being investigated to our
506 knowledge. One of the few studies describing Li-isotope values in Fe–Mn oxides is that of You
507 and Chan (1996), giving δ^7Li values between +22.9 and +33.4‰ for hydrothermal
508 ferromanganese crusts, such values being controlled by post-depositional exchange with
509 seawater. To overcome this lack, we can use data from the labile fraction extracted from soils
510 and river sediments in the same catchment (Négrel and Roy, 2002; Négrel and Petelet-Giraud,
511 2012). These were obtained by leaching with cold and dilute acid, which releases the total
512 inventory of non-residual trace elements, particularly those associated with hydrous Fe–Mn

oxides adsorbed on clays, and occurring in carbonates and sulphides in the sediment load, as well as in natural organic matter. The content of the labile sample fractions from this study is consistently low, with similar ranges in soil and sediment (0.8–10.1% of total matter content; mean 6.4%). The Mn contents of this labile fraction range between 50 and 30,000 µg/g (mean ±6,000 µg/g). In addition, strong Li-Fe and Li-Mn correlations exist in agricultural soil at a European scale (GEMAS Project; Négrel et al., 2018). This is strongly related to precipitation of Fe-Mn oxide/hydroxide coatings, which provides a control over the lithium content within such phases that encourages investigating the labile fractions in soil and sediment for Li isotopes to evaluate Li isotope fractionation during the formation of Fe-Mn oxides.

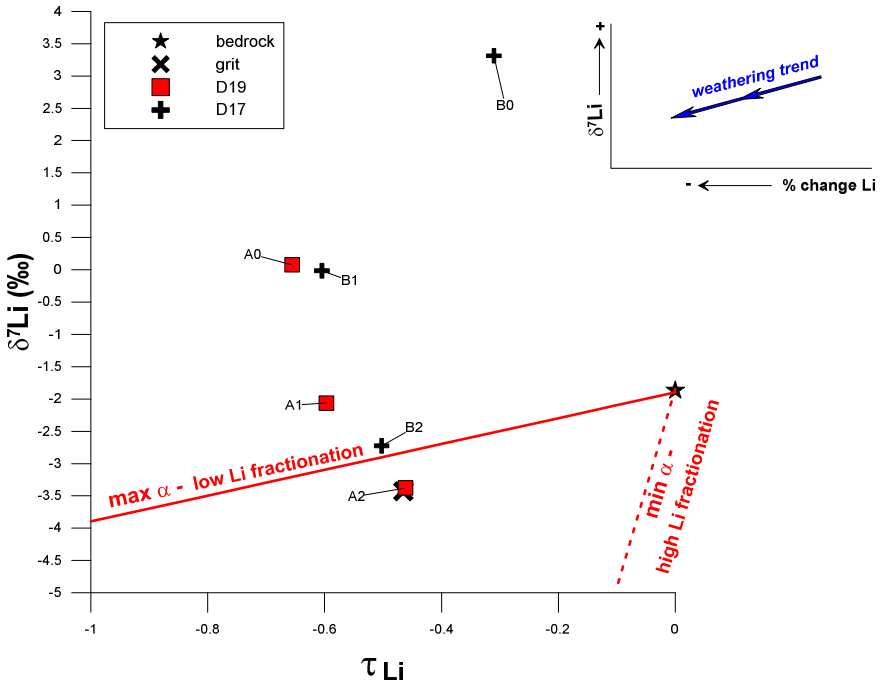

Figure 7. Li isotopic composition of surface saprolite (A0, B0), riverbank sediments (A1, B1) and soil samples (A2, B2) as a function of τLi (Equation 1). Straight lines represent the evolution of δ^7Li vs. τLi given by the batch equilibrium model according to Equation 3.

The Margeride data can be compared with other granite areas, but studies on granite and associated weathering products are relatively rare (Rudnick et al., 2004; Lemarchand et al., 2010), only the latter concerning the same type of granite as the Margeride. It presents analyses of Li concentrations and isotopic compositions in rock, soil, vegetation, soil water, rainfall, springs and stream water of the Strengbach catchment. This forested catchment in the Vosges

Mountains (NE France) has been intensively studied and monitored for decades by the University of Strasbourg. The bedrock is a leucogranite affected by hydrothermal alteration, the weathering products being saprolite (≤10 m thick) and soil overlying the saprolite (±80 cm thick). Fractionation factors $\alpha_{sec\text{-}dis}$ are illustrated on Figure 8 for the Strengbach catchment with the Margeride data (Fig. 7).

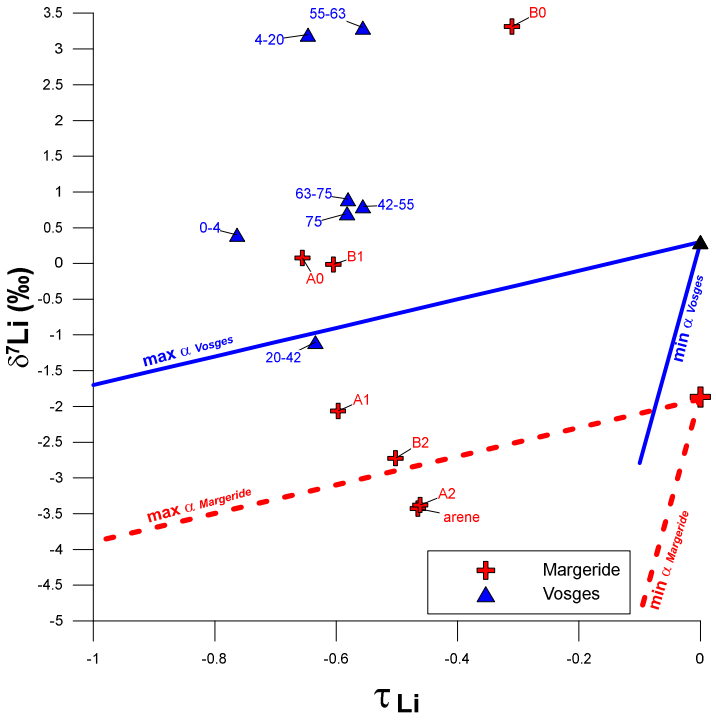

Figure 8. Comparison of Li isotopic composition of soil samples as a function of τLi for the Margeride catchment (this study, Fig. 7) and the Strengbach granitic catchment (Vosges Mountains, France; Lemarchand et al., 2010). For the latter, the numbering indicates the depth interval considered in the profile.

Again, the fractionation factor does not explain most Strengbach data. Only one weathering product can be explained considering the α max of 0.998 (low Li-isotopic fractionation) and no points are explained by the α min of 0.975 (high fractionation). Lemarchand et al. (2010) argued that soil is a strongly reactive compartment for Li isotopes, and that another phase inducing Li-isotope fractionation must be suspected. Identifying the origin of this fractionation will require more studies at catchment scale for understanding the processes at the biosphere interface. Anderson et al. (1988) demonstrated that exchangeable Li

551 is an insignificant part of the total Li present in soil, and Reimann et al. (2014a; b) showed a
552 weak affinity of Li for phases like clay and organic matter using Mobile Metal Ion (MMI®)
553 extraction. Combining sequential extraction with Li isotope measurements can help explore
554 how Li is bounded to the different mineral phases and identify the phases that cause the
555 fractionation in soil and sediment.

556 6 – Conclusions

557 We carried out a systematic study of lithium-isotope compositions of surface- and ground-
558 waters, and soil and sediment samples collected from a granite catchment in the French Massif
559 Central. This work incorporates many novel aspects, being an integrated investigation of
560 weathering processes by means of lithium isotopes.

561 In water, the lithium isotope composition (δ^7Li) of a dissolved load is generally higher
562 than corresponding δ^7Li values for groundwater, bedrock and sediment. It has been suggested
563 that Li-isotope fractionation in the dissolved load records silicate weathering intensity, as well
564 as fluid-residence time, or exchange processes between water and sediment. In soil and
565 sediment, Li is enriched through fractionation into the lithium-6 and -7 isotopes, leading to less
566 negative δ^7Li values and to changes in mineral abundance in the samples.

567 A model for determining the δ^7Li of water after interaction with granite was applied,
568 based on the assumption that Li derives from plagioclase, K-feldspar, apatite and biotite. The
569 model calculations showed a relative agreement between the Li isotope composition predicted
570 by the weathering model and that observed in water.

571 The fractionation process during granite weathering was investigated through non-
572 congruent dissolution of the bedrock, leading to a δ^7Li in solution. The main process caused by
573 this solution is the fractionation of Li isotopes through the formation of secondary phases that
574 preferentially incorporate light lithium (^{6}Li). This gives a residual solution with a specific δ^7Li
575 and another δ^7Li value for the secondary phases.

We modelled weathering products with a fractionation factor that is consistent with the range of values found in the literature. Our results show that some, but not all, weathering products can be explained by such fractionation. Additional processes or inputs must therefore be investigated, such as the precipitation of another phase with a higher isotope fractionation rate, for which Fe-Mn oxides are a good candidate. Data from the Margeride were compared with those from the Strengbach granite catchment in the Vosges Mountains (NE France); again, the fractionation factor did not explain most Strengbach data and, here too, the role of another phase was suspected.

We highlighted the possible role of Li isotopes as tracers of water-rock interaction in a granite catchment. When evaluating regolith (soil and sediment) formation, any additional tracers to the basic ones (major- and trace elements, and Sr isotopes) are important for constraining the whole weathering system.

A remaining problem to be solved concerns the distinction between primary effects related to source/origin, and the effects of secondary processes (alteration, dissolution, precipitation) that can modify the isotopic signature, and are key reactions for fractionating Li isotopes. Another approach to understanding and interpreting the isotopic signatures will require Reactive Transport Model (RTM) computer simulations, to arrive at simultaneous solution of the governing equations for solute and geochemical transformations.

Acknowledgements

This work was financially supported by the BRGM Research Division 'Isotopes' research programmes, and benefited from collaboration by the BRGM Chemistry laboratories for major- and trace element analyses: T. Conte is thanked for his assistance, as well as M. Robert for her help in the Neptune laboratory. Financial support from the Région Centre is acknowledged for acquisition of the Neptune MC-ICP-MS. We are grateful to Dr. H.M. Kluijver for proofreading and editing the English text. Paul Tomascak, two anonymous reviewers and Editor-in-Chief Karen Johannesson are warmly thanked for

their critical comments and constructive reviews that greatly improved the manuscript, and for proofreading and editing the English text. This paper is dedicated to the memory of our wonderful colleague and friend, Dr. Tom Bullen, who recently passed away (Shouakar-Stash et al., 2018).

References

Abbas, N., Subramanian, V. 1984. Erosion and sediment transport in the Ganges river basin (India). J. Hydrol., 69 173-182.

Ackerer, J., Chabaux, F., van der Woerd, J., Viville, D., Pelt, E., Kali, E., Lerouge, C., Ackerer, P., di Chiara Roupert, R, Négrel, Ph. 2016. Regolith evolution on the millennial timescale from combined U–Th–Ra isotopes and in situ cosmogenic ^{10}Be analysis in a weathering profile (Strengbach catchment, France). Earth Planet. Sci. Lett., 453, 33-43.

Amiotte Suchet, P., Probst, J.L., Ludwig, W. 2003. Worldwide distribution of continental rock lithology: Implications for the atmospheric/soil CO_2 uptake by continental weathering and alkalinity river transport to the oceans. Global Biogeochemical Cycles, 17(2).

Anderson, M.A., Bertsch, P.M., Miller, W.P. 1988. The distribution of lithium in selected soils and surface waters of the southeastern USA. App. Geochem., 3, 205-212.

Begonha, A., Sequeira Braga, M.A., 2002. Weathering of the Oporto granite: geotechnical and physical properties. Catena, 49, 57-76.

Bouchez J., von Blanckenburg F., Schuessler J.A. 2013. Modeling novel stable isotope values in the weathering zone. Am. J. Sci., 313, 267–308.

Braga, M.S., Paquet, H., Begonha, A. 2002. Weathering of granites in a temperate climate (NW Portugal): granitic saprolites and arenization. Catena, 49, 41-56.

Brimhall, G.H., Dietrich, W.E. 1987. Constitutive mass balance relations between chemical composition, volume, density, porosity, and strain in metasomatic hydrochemical systems: results on weathering and pedogenesis. Geochim. Cosmochim. Acta, 51, 567-587.

Carpenter R.H., Pope T.A., Smith R.L. 1975. Fe-Mn oxide coatings in stream sediment geochemical surveys. J. Geochem. Expl., 4, 349-363.

Clergue, C., Dellinger, M., Buss, H.L., Gaillardet, J. Benedetti, M.F., Dessert C. 2015. Influence of atmospheric deposits and secondary minerals on Li isotopes budget in a highly weathered catchment, Guadeloupe (Lesser Antilles). Chem. Geol., 414, 28-41.

Dellinger, M., Gaillardet, J., Bouchez, J., Calmels, D., Louvat, P., Gorge, C., Maurice, L., 2013. Lithium isotopic composition of the dissolved load in the Amazon River Basin. Mineral. Mag., 77, 967.

Dellinger, M., Gaillardet, J., Bouchez, J., Calmels, D., Galy, V., Hilton, R. G., Louvat, P. France-Lanord, C. 2014. Lithium isotopes in large rivers reveal the cannibalistic nature of modern continental weathering and erosion. Earth Planet. Sci. Lett., 401, 359–372.

637 Dellinger, M., Gaillardet, J., Bouchez, J., Calmels, D., Louvat, P., Dosseto, A., Gorge, C., Alanoca, L.,
638 Maurice, L. 2015. Riverine Li isotope fractionation in the Amazon River basin controlled by the
639 weathering regimes. Geochim. Cosmochim. Acta, 164, 71–93.
640 Gaillardet, J., Dupré, B., Louvat, P., Allègre, C.J. 1999. Global silicate weathering and CO_2 consumption
641 rates deduced from the chemistry of the large rivers, Chem. Geol., 159, 3–30.
642 Grosbois, C., Négrel, Ph., Fouillac, C., Grimaud, D. 2000. Dissolved load of the Loire River: chemical
643 and isotopic characterization. Chem. Geol., 170, 179-201.
644 Harlavan, Y., Erel, Y., 2002. The release of Pb and REE from granitoids by the dissolution of accessory
645 phases. Geochim. Cosmochim. Acta, 66, 837–848.
646 Hathorne, E.C., James, R. H. 2006. Temporal record of lithium in seawater: A tracer for silicate
647 weathering?. Earth Planet. Sci. Lett., 246, 393-406.
648 Henchiri, S., Gaillardet, J., Dellinger, M., Bouchez, J., Spencer, R.G.M. 2016. Riverine dissolved
649 lithium isotopic signatures in low-relief central Africa and their link to weathering regimes. Geophys.
650 Res. Lett., 43, doi:10.1002/2016GL067711.
651 Henchiri S., Clergue C., Dellinger M., Gaillardet J., Louvat P. Bouchez J. 2014. The influence of
652 hydrothermal activity on the Li isotopic signature of rivers draining volcanic areas. Proc. Earth
653 Planet. Sci., 10, 223–230.
654 Huh, Y., Chan, L.H., Zhang, L., Edmond, J.M. 1998. Lithium and its isotopes in major world rivers:
655 Implications for weathering and the oceanic budget. Geochim. Cosmochim. Acta, 62, 2039-2051.
656 Huh, Y., Chan, L.H., Edmond, J.M. 2001. Lithium isotopes as a probe of weathering processes: Orinoco
657 River. Earth Planet. Sci. Lett., 194, 189-199.
658 Huh, Y, Chan, L.H., Zhang, L., Edmond, J.M. 1998. Lithium and its isotopes in major world rivers:
659 Implications for weathering and the oceanic budget. Geochim. Cosmochim. Acta, 62, 2039–2051.
660 Huh, Y., Chan, L.H., Chadwick, O.A. 2004. Behavior of lithium and its isotopes during weathering of
661 Hawaiian basalt. Geochem. Geoph. Geosyst., 5(9), 1-22.
662 Kisakurek, B., Widdowson, M., James, R.H. 2004. Behaviour of Li isotopes during continental
663 weathering: the Bidar laterite profile, India. Chem. Geol., 212, 27-44.
664 Kisakurek, B., James, R.H., Harris, N.B.W. 2005. Li and δ^7Li in Himalayan rivers: Proxies for silicate
665 weathering? Earth Planet. Sci. Lett., 237, 387– 401
666 Le Pera, E., Critelli, S., Sorriso-Valvo, M. 2001. Weathering of gneiss in Calabria, southern Italy.
667 Catena, 42, 1-15.
668 Liu, C.Q., Zhao, Z.Q., Wang, Q., Gao, B. 2011. Isotope compositions of dissolved lithium in the rivers
669 Jinshajiang, Lancangjiang, and Nujiang: Implications for weathering in Qinghai-Tibet Plateau. App.
670 Geochem., 26, S357-S359.
671 Liu, X.M. Wanner, C., Rudnick, R.L., McDonough, W.F. 2015. Processes controlling δ^7Li in rivers
672 illuminated by study of streams and groundwaters draining basalts. Earth Planet. Sci. Lett., 409, 212-
673 224.

Lemarchand, E. Chabaux, F., Vigier, N., Millot, R. Pierret, M.C. 2010. Lithium isotope systematics in a forested granitic catchment (Strengbach, Vosges Mountains, France). Geochim. Cosmochim. Acta, 74, 4612–4628.

Meybeck, M., 1983. Atmospheric inputs and river transport of dissolved substances. IAHS Publ., 141, 173–192.

Millot, R., Guerrot, C., Vigier, N. 2004. Accurate and high precision measurement of lithium isotopes in two reference materials by MC-ICP-MS. Geostandards and Geoanalytical Res., 28, 153-159.

Millot, R., Vigier, N., Gaillardet, J. 2010a. Behaviour of lithium and its isotopes during weathering in the Mackenzie Basin, Canada. Geochim. Cosmochim. Acta, 74, 3897–3912.

Millot, R., Petelet-Giraud, E., Guerrot, C., Négrel, Ph. 2010b. Multi-isotopic composition (δ^{7}Li-δ^{11}B-δD-δ^{18}O) of rainwaters in France: Origin and spatio-temporal characterization. Appl. Geochem., 25, 1510-1524.

Millot, R., Scaillet, B., Sanjuan, B. 2010c. Lithium isotopes in island arc geothermal systems: Guadeloupe, Martinique (French West Indies) and experimental approach. Geochim. Cosmochim. Acta, 74, 1852–1871.

Millot, R., Négrel, Ph., Petelet-Giraud, E. 2007. Multi-isotopic (Li, B, Sr, Nd) approach for geothermal reservoir characterization in the Limagne Basin (Massif Central, France). Appl. Geochem., 22, 2307-2325.

Millot, R., Négrel, Ph. 2007. Multi-isotopic tracing (δ^{7}Li, δ^{11}B, ^{87}Sr/^{86}Sr) and chemical geothermometry: evidence from hydro- geothermal systems in France. Chem. Geol., 244, 664-678.

Millot, R., Négrel, Ph. 2013. Chemical weathering of granitic rocks: experimental approach and Pb-Li isotopes tracing. Proc. Earth Planet. Sci., 7, 590-593.

Millot, R., Tremosa, J., Négrel, Ph. 2019. Chemical weathering of a granitic watershed: coupling Lithium isotopes and reactive transport modeling, preliminary results. WRI-16, Tomsk, Russia, July 21-26 2019.

Murphy, M.J., Porcelli, D., von Strandmann, P.A.E., Hirst, C.A., Kutscher, L., Katchinoff, J.A., Mörth, C.M., Maximov, T., Andersson, P.S. 2019. Tracing silicate weathering processes in the permafrost-dominated Lena River watershed using lithium isotopes. Geochim. Cosmochim. Acta, 245, 154-171.

Négrel, Ph., Casanova, J., Aranyossy, J.F. 2001. Strontium isotope systematics used to decipher the origin of groundwaters sampled from granitoids: the Vienne case (France). Chem. Geol., 177, 287-308.

Négrel, Ph, Allègre, C.J., Dupré, B., Lewin, E. 1993. Erosion sources determined from inversion of major, trace element ratios and strontium isotopic ratios in river water: the Congo Basin case. Earth Planet Sci. Lett., 120, 59–76.

Négrel, Ph., Guerrot, C., Cocherie, A., Azaroual, M., Brach, M., Fouillac, C. 2000. Rare Earth Elements, neodymium and strontium isotopic systematics in mineral waters: evidence from the Massif Central, France. Appl. Geochem., 15, 1345-1367.

Negrel, Ph., Fouillac, C., Brach, M. 1997. Occurrence of mineral water springs in the stream channel of the Allier River (Massif Central, France): Chemical and Sr isotope constraints. J. Hydrol., 203, 143-153.

Négrel, Ph. 1999. Geochemical study of a granitic area – The Margeride Mountains, France: chemical element behavior and $^{87}Sr/^{86}Sr$ constraints. Aq. Geochem., 5, 125–165.

Négrel, Ph. 2006. Water-granite interaction: clues from strontium, neodymium and rare earth elements in saprolite, sediments, soils, surface and mineralized waters. Appl. Geochem., 21, 1432-1454.

Négrel, Ph., Millot, R., Brenot, A., Bertin, C. 2010a. Lithium isotopes as tracers of groundwater circulation in a peat land. Chem. Geol., 276, 119-127.

Négrel, Ph., Millot, R., Roy, S., Guerrot, C., Pauwels, H. 2010b. Lead isotopes in groundwater as an indicator of water–rock interaction (Masheshwaram catchment, Andhra Pradesh, India). Chem. Geol., 274 136–148.

Négrel, Ph., Roy, S., 1998. Rain chemistry in the Massif Central (France). A strontium isotopic and major elements study. App. Geochem. 13, 941–952.

Négrel, Ph., Roy, S. 2002. Investigating the sources of the labile fraction in sediments from silicate-drained rocks using trace elements, and strontium and lead isotopes. Sci. Tot. Env., 298, 163-181.

Négrel, Ph., Pauwels, H., Chabaux, F. 2018. Characterizing multiple water-rock interactions in the critical zone through Sr-isotope tracing of surface and groundwater. Appl. Geochem., 93, 102-112.

Négrel, Ph., Petelet-Giraud, E. 2012. Isotopic evidence of lead sources in Loire River sediment. Appl. Geochem., 27, 2019-2030.

Négrel Ph, Millot R, Guerrot C, Petelet-Giraud E, Brenot A, Malcuit E. 2012. Heterogeneities and interconnections in groundwater: coupled B, Li and stable isotope variations in a large aquifer system (France). Chem. Geol., 296-297, 83–95.

Négrel, Ph., Ladenberger A., Reimann, C., Birke, M., Demetriades, A., Sadeghi, M. 2018. Low-density geochemical mapping at continental scale reveals background for emerging tech-critical elements. Geoph. Res. Abstr., 20, EGU2018-18573, EGU General Assembly Vienna 2018.

Nesbitt, H.W., Markovics, G. 1980. Chemical processes affecting alkalis and alkaline earths during continental weathering. Geochim. Cosmochim. Acta, 44, 1659-1666.

Nesbitt, H.W. 1979. Mobility and fractionation of rare earth elements during weathering of a granodiorite. Nature, 279, 206–210.

Paquet, H., Clauer, N. (Eds.). 2012. Soils and Sediments: Mineralogy and Geochemistry. Springer Science & Business Media, XYZ p.

Petelet-Giraud, E., Négrel, Ph., Casanova, J., 2003. Variability of $^{87}Sr/^{86}Sr$ in water draining granite revealed after a double correction for atmospheric and anthropogenic inputs. Hydrol. Sci. J., 48, 729-742.

Pistiner, J.S., Henderson G.M. 2003. Lithium-isotope fractionation during continental weathering processes. Earth Planet. Sci. Lett., 214, 327-339.

748 Pogge von Strandmann P.A.E., Burton K., James R., van Calsteren P. Gislason S. 2010. Assessing the
749 role of climate on uranium and lithium isotope behaviour in rivers draining a basaltic terrain. Chem.
750 Geol., 270, 227–239.
751 Pogge von Strandmann, P.A.E., Opfergelt, S., Lai, Y.J., Sigfusson, B., Gislason, S.R., Burton, K.W.
752 2012. Lithium, magnesium and silicon isotope behavior accompanying weathering in a basaltic soil
753 and pore water profile in Iceland. Earth Planet. Sci. Lett., 339–340, 11-23.
754 Pogge von Strandmann, P.A.E., Porcelli, D., James, R.H., van Calsteren, P., Schaefer, B., Cartwright,
755 I., Reynolds, B.C., Burton, K.W. 2014. Chemical weathering processes in the Great Artesian Basin:
756 Evidence from lithium and silicon isotopes. Earth Planet. Sci. Lett., 406, 24-36.
757 Pogge von Strandmann, P.A.E., Fraser, W.T., Hammond, S.J., Tarbuck, G., Wood, I.G., Oelkers, E.H.,
758 Murphy, M.J. (2019). Experimental determination of Li isotope behaviour during basalt weathering.
759 Chem. Geol. https://doi.org/10.1016/j.chemgeo.2019.04.020.
760 Reimann, C., Birke, M., Demetriades, A., Filzmoser, P., O'Connor, P. 2014a. Chemistry of Europe's
761 Agricultural Soils, Part A: Methodology and Interpretation of the GEMAS Dataset. Geologisches
762 Jahrbuch (Reihe B). Schweizerbarth, Stuttgart, 528 p.
763 Reimann, C., Birke, M., Demetriades, A., Filzmoser, P., O'Connor, P. 2014b. Chemistry of Europe's
764 Agricultural Soils–Part B: General Background Information and Further Analysis of the GEMAS
765 Dataset. Geologisches Jahrbuch (Reihe B). Schweizerbarth, Stuttgart, 352 p.
766 Rudnick, R.L., Tomascak, P.B., Njo, H.B., Gardner, L.R. 2004. Extreme lithium isotopic fractionation
767 during continental weathering revealed in saprolites from South Carolina. Chem. Geol., 212, 45-57.
768 Ryu, J.S., Vigier, N., Lee, S.W., Lee, K.S. Chadwick, O.A. 2014. Variation of lithium isotope
769 geochemistry during basalt weathering and secondary mineral transformations in Hawaii. Geochim.
770 Cosmochim. Acta, 145, 103-115.
771 Sequeira Braga, M.A., Lopes Nunes, J.E., Paquet, H., Millot, G. 1990. Climatic zonality of coarse
772 granitic saprolites ("arènes") in Atlantic Europe from Scandinavia to Portugal. Sciences Géologiques,
773 Bulletins et Mémoires, 85, 99-108.
774 Sequeira Braga, M.S., Paquet, H., Begonha, A. 2002. Weathering of granites in a temperate climate
775 (NW Portugal): Granitic saprolites and arenization. Catena, 49, 41-56.
776 Sarazin, G., 1979. Géochimie de l'aluminium au cours de l'altération des granites et basaltes sous climat
777 tempéré. Doctoral thesis, University of Paris VI, 169 p.
778 Shouakar-Stash, O., Kharaka, Y., Koopmann, R., Harmon, R., Négrel, Ph., Wanty, R.B. 2018. A
779 remembrance of Thomas (Tom) Bullen, 1951-2018. Appl. Geochem., 98, 474-475.
780 Stallard, R.F., Edmond, J.M. 1981. Geochemistry of the Amazon: 1. Precipitation chemistry and the
781 marine contribution to the dissolved load at the time of peak discharge. J. Geophys. Res.: Oceans,
782 86(C10), 9844-9858.
783 Sullivan, P.L., Ma, L., West, N., Jin, L., Karwan, D.L., Noireaux, J., Steinhoefel, G., Gaines, K.P.,
784 Eissenstat, D.M., Gaillardet, J., Derry L.A., Meek, K., Hynek S., Brantley S.L. 2016. CZ-tope at

785 Susquehanna Shale Hills CZO: Synthesizing multiple isotope proxies to elucidate Critical Zone
786 processes across timescales in a temperate forested landscape. Chem. Geol., 445, 103-119.
787 Tsai, P.H., You, C.F., Huang, K.F., Chung, C. H., Sun, Y.B. 2014. Lithium distribution and isotopic
788 fractionation during chemical weathering and soil formation in a loess profile. J. Asian Earth Sci.,
789 87, 1-10.
790 Tomascak, P.B. 2004. Developments in the understanding and application of lithium isotopes in the
791 earth and planetary sciences. Rev. Mineral. Geochem., 55, 153-195.
792 Vázquez M., Ramírez S., Morata D., Reich M., Braun J.J., Carretier S. 2016. Regolith production and
793 chemical weathering of granitic rocks in central Chile. Chem. Geol., 446, 87-98.
794 Velbel, M.A. 1988. Weathering and soil-forming processes. In: Forest Hydrology and Ecology at
795 Coweeta. Springer, New York, NY, 93-102.
796 Vigier, N., Decarreau, A., Millot, R., Carignan, J., Petit, S. France-Lanord, C. 2008. Quantifying Li
797 isotope fractionation during smectite formation and implications for the Li cycle. Geochim.
798 Cosmochim. Acta, 72, 780–792.
799 Vigier, N., Gislason, S.R., Burton, K.W., Millot, R., Mokadem, F. 2009. The relationship between
800 riverine lithium isotope composition and silicate weathering rates in Iceland. Earth Planet. Sci. Lett.,
801 287, 434–441.
802 Wanner, C., Bucher, K. Pogge von Strandmann P.A.E., Waber, H.N. Pettke T. 2017. On the use of Li
803 isotopes as a proxy for water–rock interaction in fractured crystalline rocks: A case study from the
804 Gotthard rail base tunnel. Geochim. Cosmochim. Acta, 198, 396-418.
805 Wang, Q.L., Chetelat, B., Zhao, Z.Q., Ding, H., Li, S.L., Wang, B.L., Li, J., Liu, X.L. 2015. Behavior
806 of lithium isotopes in the Changjiang River system: Sources effects and response to weathering and
807 erosion. Geochim. Cosmochim. Acta, 151, 117–132.
808 Weynell, M., Wiechert, U., Schuessler, J.A. 2017. Lithium isotopes and implications on chemical
809 weathering in the catchment of Lake Donggi Cona, northeastern Tibetan Plateau. Geochim.
810 Cosmochim. Acta, 213, 155-177.
811 White, A.F., Blum, A.E. 1995. Effects of climate on chemical weathering in watersheds. Geochim.
812 Cosmochim. Acta, 59, 1729-1747.
813 Wimpenny, J., Gislason, S.R., James, R.H., Gannoun, A., Pogge von Strandmann, P.A.E, Burton, K.W.
814 2010. The behaviour of Li and Mg isotopes during primary phase dissolution and secondary mineral
815 formation in basalt. Geochim. Cosmochim. Acta, 74, 5259-5279.
816 You, C.F., Chan, L.H. 1996. Precise determination of lithium isotopic composition in low concentration
817 natural samples. Geochim. Cosmochim. Acta, 60, 909-915.
818

Sample	**Ref.**	Li µg g-1	δ7Li
M1/POU	Whole rock	143.1	-1.9
ALT1	Mazel grit	104.7	-3.4
Ap	Apatite	13.3	0.0
Pl	Plagioclase	20.9	-1.7
Bi	Biotite	489.1	0.8
KF	K-Feldspar	5.3	-2.6
D19-3/A0	A0	56.2	0.1
D19-3/A1	A1	68.8	-2.1
D19-3/A2	A2	110.9	-3.4
D17-3/B0	B0	60.6	3.3
D17-3/B1	B1	61.6	0.0
D17-3/B2	B2	66.2	-2.7

Sample	Li µmol L-1	δ7Li
Spring waters		δ7Li
Mazel	551	5.0
FB1	424	4.9
Ranc1	158	3.8
Ranc2	397	2.6
Surface waters		
D10'	0.22	12.7
D8	0.15	9.2
D11	0.23	12.1
D9bis	0.16	10.0
D9'	0.21	10.7
D11'	0.24	13.0